FULL PAPER

A Solution-Processed UV-Sensitive Photodiode Produced Using a New Silicon Nanocrystal Ink

*Tao Lin, Xin Liu, Bin Zhou, Zhiyong Zhan, Alexander N. Cartwright, and Mark T. Swihart**

This article presents a simple and effective method of functionalizing hydrogen-terminated silicon (Si) nanocrystals (NCs) to form a high-quality colloidal Si NC ink with short ligands that allow charge transport in nanocrystal solid films. Si NCs fabricated by laser-pyrolysis and acid etching are passivated with allyl disulfide via ultraviolet (UV)-initiated hydrosilylation to form a stable colloidal Si NC ink. Then a Si NC-based photodiode is directly fabricated in air from this ink. Only a solution-processed poly(3,4-ethylenedioxy-thiophene):poly(styrene sulfonate) (PEDOT: PSS) electron blocking layer and top- and bottom-contacts are needed along with the Si NC layer to construct the device. A Schottky-junction at the interface between the Si NC absorber layer and aluminum (Al) back electrode drives charge separation in the device under illumination. The unpackaged Si NC-based photodiode exhibites a peak photoresponse of 0.02 A W^{-1} to UV light in air, within an order of magnitude of the response of commercially available gallium phosphide (GaP), gallium nitride (GaN), and silicon carbide (SiC) based photodetectors. This provides a new pathway to large-area, low-cost solution-processed UV photodetectors on flexible substrates and demonstrates the potential of this new silicon nanocrystal ink for broader applications in solution-processed optoelectronics.

1. Introduction

Colloidal nanocrystals (NCs) are promising materials for next generation optoelectronic devices including light-emitting diodes (LEDs),[1] photovoltaic devices (PV),[2] and photodetectors.[3] The promise of these materials arises from both the potential benefits of quantum size effects and the practical advantages of solution-phase processing.[4] Quantum size effects enable tuning of both the absorption onset and emission wavelength of NCs over a wide range, while solution-phase printing and coating processes enable large device area, use of low-cost and flexible substrates, and reduced costs in device fabrication compared to conventional vacuum processing.[5] However, to date, the most promising NC devices have incorporated toxic heavy metals, such as cadmium, lead, and mercury. Concerns have been raised about the risks that these materials pose to human health and to the environment. Such concerns are avoided in devices made from silicon (Si) NCs. Silicon is abundant and non-toxic, and is the dominant material used throughout the microelectronics and PV industries. Building upon recent advances in the synthesis of high quality silicon NCs with controlled size, shape, and surface chemistry,[6] silicon is now poised to play an important role in a new generation of low-cost, high-performance optoelectronic devices.[1c,3c,7]

The band-gaps of colloidal silicon NCs are determined by both size-dependent quantum confinement effects and by the nature of the silicon surface. Silicon NCs are typically capped with long organic ligands that prevent aggregation of particles, stabilize them against oxidation, and allow formation of stable high-concentration dispersions (inks) in organic solvents. These properties allow the NCs to be used in solution-based device fabrication. Unfortunately, ligands with long hydrocarbon chains, such as octadecene or ethyl undecylenate, may block interparticle charge carrier transport, which results in exceedingly low charge mobility in solid films of the particles.[1d,8] However, direct synthesis of NCs passivated by short ligands is often ineffective in preventing NC aggregation, resulting in formation of rough, cracked, porous, or otherwise defective NC films fabricated from colloidal NC inks. The solid-state ligand-exchange strategies that are commonly applied to improve charge mobility in II–VI[9] and IV–VI[2f,10] NC thin films cannot generally be used with silicon NC films, because the ligands on silicon NCs are typically attached by strong covalent bonds. These strong covalent bonds are desirable for providing robust protection against oxidation, but have the disadvantage of precluding ligand exchange in cast films. Kortshagen's group

Dr. T. Lin, Dr. X. Liu, Prof. M. T. Swihart
Department of Chemical and Biological Engineering
University at Buffalo (SUNY)
Buffalo, New York 14260, USA
E-mail: swihart@buffalo.edu
Dr. T. Lin
National Laboratory of Solid State Microstructures
School of Electronic Science
and Engineering and School of Physics
Nanjing University
Nanjing 210093, China
Dr. B. Zhou, Z. Zhan, Prof. A. N. Cartwright
Department of Electrical Engineering
University at Buffalo (SUNY)
Buffalo, New York 14260, USA

DOI: 10.1002/adfm.201400600

© 2014 WILEY-VCH Verlag GmbH & Co. KGaA, Weinheim

found that chlorine-terminated plasma-synthesized silicon nanoparticles can disperse well in ketones and nitriles. They attribute this to hypervalent interactions of these molecules with the chlorine-terminated silicon surface.[11] Our group similarly showed that hydrogen-terminated silicon-germanium alloy NCs formed stable colloids in benzonitrile after sonication for an extended time.[12] These advances suggested an alternative strategy for producing colloidally stable Si NC inks suitable for device applications. However, a drawback of this approach was the high sensitivity to oxidation of films cast from these bare (Cl- or H- terminated) Si NC inks. Here, we present a method for formation of a Si NC ink with high air stability that can directly produce Si NC films with high conductivity. We then demonstrate a solution-processed UV-sensitive photodiode prepared using this Si NC ink.

2. Results and Discussion

2.1. Preparation and Functionalization of Colloidal Si NCs

A schematic diagram of the process for preparing the Si NC ink is shown in **Figure 1**. Bare silicon NCs were produced by laser-induced pyrolysis of silane, as described in detail previously.[6b] The resulting NCs were etched with a mixture of hydrofluoric acid (HF) and nitric acid (HNO_3) to reduce the particle size and provide an oxygen-free hydrogen-terminated surface. The particle size, and therefore the band gap, can be controlled by varying the etching time. The next step, and the key challenge in producing solution-processed Si NC devices, is to functionalize the Si NCs with appropriate ligands that allow formation of stable Si NC dispersions without overly diminishing the conductivity of Si NC solid films cast from those dispersions. We have used several short ligands, including acrylic acid, allyl alcohol and 3-buten-1-ol to functionalize Si NCs, because appreciable charge mobility in solution-processed thin films of NC passivated by such short ligands[2f,10a] has been reported for other materials. However, these have not proven effective for creating stable inks from our Si NCs. Compared to the ligands usually used in stabilizing silicon NCs, allyl disulfide has a relatively short hydrocarbon chain. Its two terminal alkene groups provide the possibility of passivating the Si NC surfaces by hydrosilylation. They also provide the possibility of forming cross-links between Si NPs (reaction mode 2 in Figure 1), either in solution or after film deposition. Both ends of an allyl disulfide molecule could also bind to the same NC (reaction mode 3 in Figure 1), though this does not seem to be the dominant binding motif, vide infra. The lone pairs of electrons in disulfide (S-S) bonds may improve the charge transport among the Si NCs relative to purely aliphatic linkages. Moreover, allyl disulfide has relatively high viscosity compared to the organic solvents most often used for solution-processing in optoelectronics, e.g., hexane, toluene, and dichlorobenzene. As a result, casting films from allyl disulfide as solvent improves

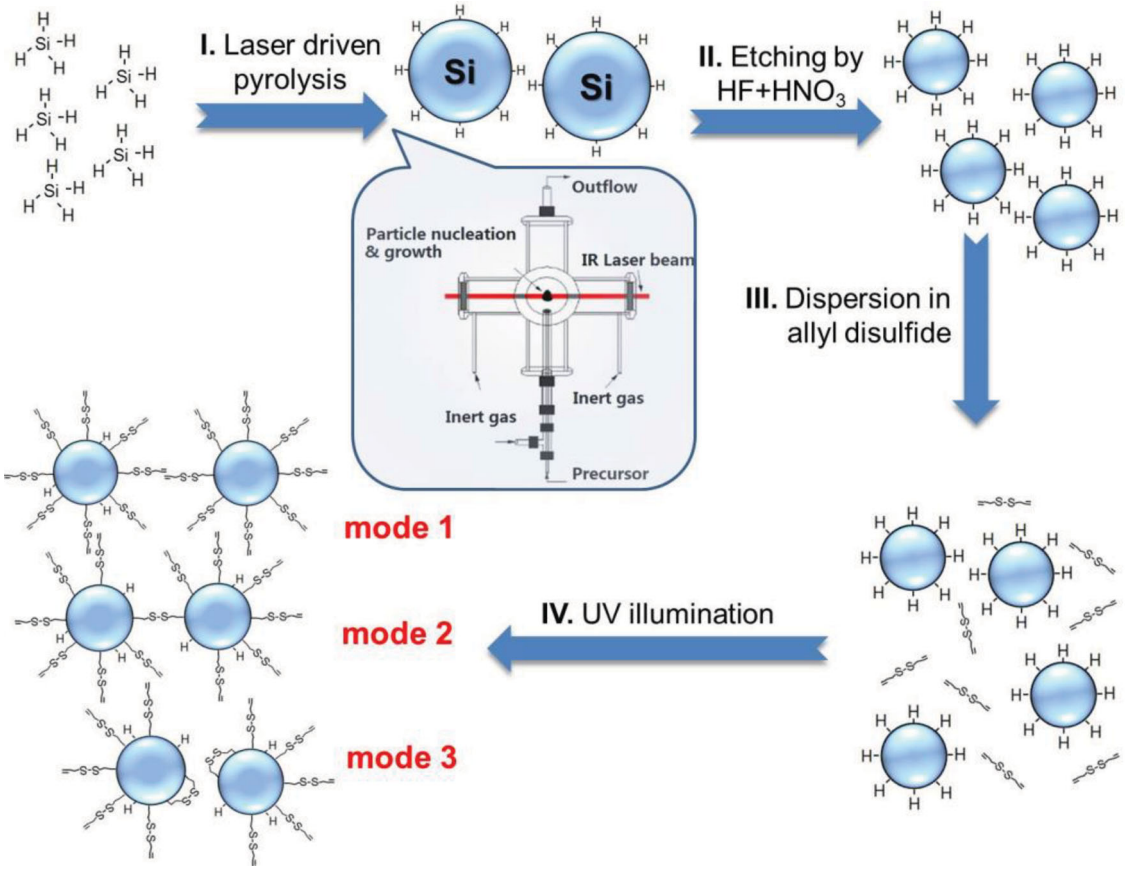

Figure 1. Schematic of the synthesis and functionalization of Si NCs.

© 2014 WILEY-VCH Verlag GmbH & Co. KGaA, Weinheim

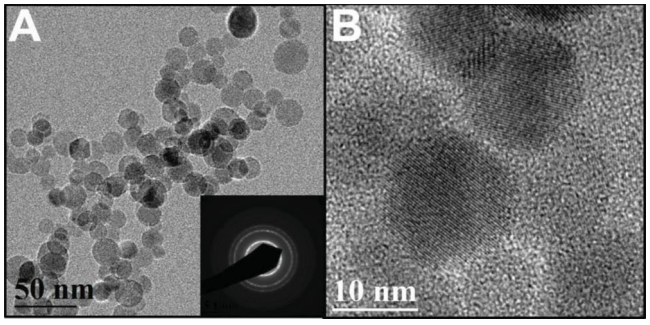

Figure 2. TEM of Si NCs synthesized by laser-driven pyrolysis, prior to HF-HNO_3 etching.

film smoothness and reduces crack formation. The moderate vapor pressure (slightly over 1 kPa at ambient conditions) of allyl disulfide also favors film formation and densification via slow evaporation. In addition, allyl disulfide occurs naturally in plants of the genus *Allium* (e.g., garlic) that are commonly used in cooking. Thus, its low toxicity and environmental compatibility are well established.

Transmission electron microscopy (TEM) showed the quasi spherical morphology and 15–20 nm size of Si NCs synthesized by laser-driven pyrolysis (**Figure 2**). An HF/HNO_3 mixture was used to etch the Si NCs to reduce their size. The etched Si NCs with a hydrogen-terminated surface could be directly dispersed in allyl disulfide at concentrations up to ≈30 mg/mL to form a Si NC ink after sonication for ≈1 min (**Figure 3**). Such a colloidal dispersion was not achieved in previous investigations of surface passivation of hydrogen-terminated Si NCs using octadecene, ethyl undecylenate, and other terminal alkenes, without UV-induced hydrosilylation. Fourier transform infrared spectroscopy (FTIR) was employed to characterize the surface state of the silicon NCs before and after reaction with allyl disulfide. The fresh silicon NC sample was removed from the nitrogen-filled glove box for FTIR measurement just after etching. This sample showed Si-H bond stretching near 2100 cm^{-1} and a small amount of Si-O and Si-O-Si bending that might arise from oxidation during the measurement (**Figure 4**, top spectrum). This demonstrates that the Si NCs have clean Si-H surfaces after etching using HF/HNO_3. To study the change in the Si NC surface upon dispersion in allyl disulfide, the Si NCs were separated from the allyl disulfide by addition of methanol

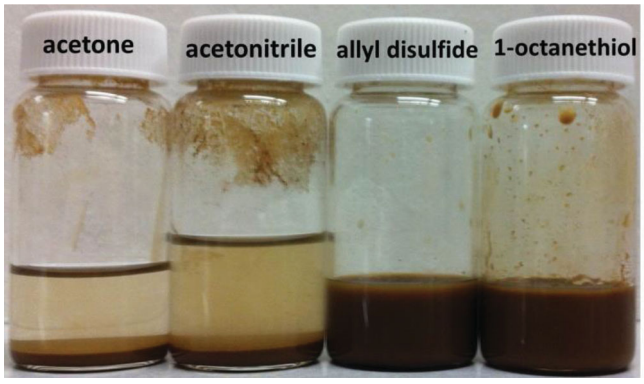

Figure 3. Bare etched (H-terminated) Si NCs dispersed in several solvents, as indicated by labels.

and centrifugation and were then washed with methanol several times to remove free allyl disulfide. FTIR showed little change of the characteristic peaks between the fresh Si NCs and the Si NCs that had been dispersed in allyl disulfide then recovered and washed (Figure 4). This indicates the absence of covalent chemical binding between Si NCs and allyl disulfide when the NCs are simply dispersed in allyl disulfide. Aggregation and precipitation of the Si NC dispersion in allyl disulfide were observed after exposure to air for several minutes, which we attribute to oxidation of the Si NC surfaces. Although these Si NC dispersions could potentially be used for making devices by coating and printing in an inert environment, they are not suitable for use in air, which is more practical for low-cost fabrication of large-area devices.

Figure 3 shows a photograph of dispersions of the Si NCs in several solvents, including acetone and acetonitrile, which have recently been shown to form stable dispersions of chlorine-terminated silicon nanocrystals.[11] Hydrogen-terminated silicon nanocrystals rapidly aggregate in, and precipitate from, these solvents. This is consistent with the fact that hypervalent interactions of silicon with ketones and nitriles requires the presence of strongly electron-withdrawing chlorine atoms on the Si NC surface. However, the H-terminated silicon nanoparticles disperse reasonably well not only in allyl disulfide, but also in thiols, such as 1-octanethiol (Figure 3). This suggests that sulfur may be interacting with the H-terminated Si NC surface. The technical grade allyl disulfide used here is of 80% purity, so interaction of the Si NC with thiol or sulfide groups, rather than the disulfide groups of allyl disulfide, cannot be ruled out as contributing to the dispersion of Si NCs in allyl disulfide. Unfortunately, interactions of thiol, sulfide, and disulfide groups with H-terminated silicon are relatively unexplored in the literature. A detailed study of the mechanism of stabilization of H-terminated Si NC colloids in allyl disulfide is beyond the scope of the present paper. Nonetheless, the observation is of considerable practical importance because it greatly simplifies the production of stable Si NC inks in allyl disulfide.

UV-induced hydrosilylation was used to covalently attach allyl disulfide to the NC surfaces and thereby stabilize the NCs against oxidation in air. The Si NC dispersion in allyl disulfide was exposed to UV light for 2 hrs. The Si NCs were then collected by adding methanol and centrifuging. They were subsequently washed with methanol to remove any residual free allyl disulfide. After UV exposure, several additional peaks were observed in the FTIR spectrum of the washed particles (Figure 4). The Si-CH_2-peak demonstrates the presence of a covalent bond between Si NC surface and allyl disulfide, confirming the occurrence of hydrosilylation under UV illumination. Moreover, the significant reduction of the Si-O-Si peak demonstrates that Si NC surface was effectively passivated by allyl disulfide and was thus resistant to oxidation in air. Ligands typically used to passivate Si NCs contain only one terminal alkene group, while allyl disulfide has two terminal alkene groups. Thus, hydrosilylation can occur between the hydrogen-terminated Si NC surface and one terminal alkene in allyl disulfide (Figure 1 reaction mode 1), but can also occur at both ends of the allyl disulfide molecule (Figure 1 reaction mode 2 and reaction mode 3). FTIR shows a strong characteristic peak at 1630 cm^{-1} corresponding to a stretching mode of the

© 2014 WILEY-VCH Verlag GmbH & Co. KGaA, Weinheim

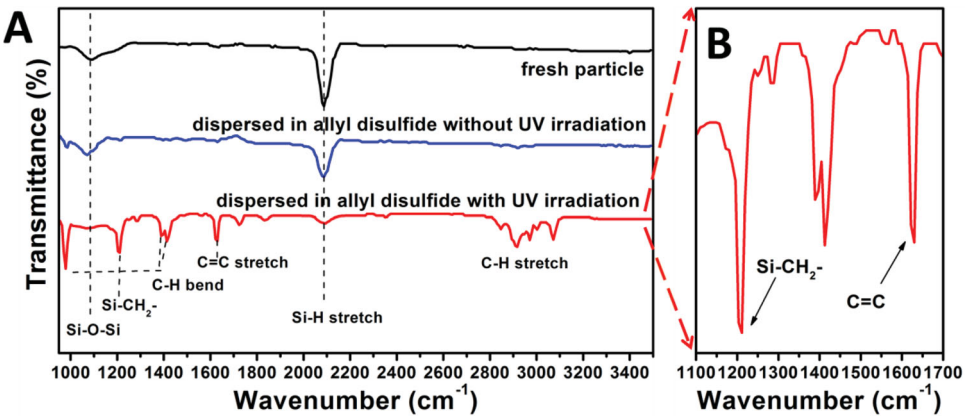

Figure 4. FTIR of fresh Si NCs (black curve), Si NCs dispersed in allyl disulfide then recovered and washed (blue curve), and Si NCs after exposure to UV illumination in allyl disulfide (red curve).

C=C bond, suggesting that much of the attachment occurs by reaction mode 1, leaving a terminal C=C bond free after hydrosilylation. The fact that the colloidal dispersion remained clear also shows that extensive cross-linking of Si NCs, via bonding by reaction mode 2, did not occur. The presence of both residual Si-H and of C=C bonds after hydrosilylation implies that further cross-linking between particles (Figure 1, reaction mode 3) may be possible after film formation, during heating and solvent evaporation.

TEM imaging showed that the etched Si NCs passivated by allyl disulfide through UV-induced hydrosilylation had a mean diameter of ≈4.5 nm (**Figure 5**A). High-resolution TEM showed lattice fringes with 0.31 nm spacing, corresponding to the (111) crystal planes of Si (Figure 5B). Powder X-ray diffraction (XRD) shows that the etched particles after disulfide passivation retain the crystal structure of the Si NCs before etching (**Figure 6**A). Moreover, the XRD peaks are slightly broadened after etching, reflecting the reduced mean size of the particles. Figure 6B shows the optical absorbance of Si NCs with a mean size of 4.5 nm. The absorbance intensity dramatically decayed in the NIR, reflecting quantum confinement in the NCs. This is consistent with previous investigations of the shift of the indirect band gap of Si NC with decreasing size.[13]

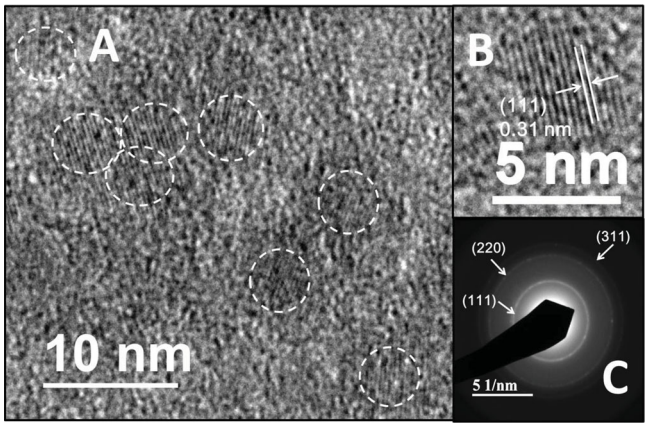

Figure 5. TEM of etched Si NCs passivated by allyl disulfide. A) Overview of several Si NCs, B) higher magnification view of a single SiNC, and C) selected area electron diffraction pattern from an area containing a large number of Si NCs. A TEM image with lower resolution is available in Figure S1 in the Supporting Information.

2.2. Solution-Processed UV Photodiode Fabricated from Si NC Ink

Solution-processing approaches for making semiconductor devices, including coating and printing, could dramatically lower cost and energy consumption of device fabrication. An important factor impacting the fabrication and performance of solution-processed devices, whether NC-based or purely organic, is the quality and stability of the solution used for fabrication. Ideally, this solution should be stable in air, so that an inert environment is not required for device fabrication. Dispersions of "bare" or H-terminated Si NCs are relatively unstable in air due to the absence of robust surface passivation. Thus, they are subject to rapid surface oxidation, and fabrication of devices from such inks must be executed under an inert environment. Moreover, protective, encapsulating layers must be deposited before the Si NC films are exposed to air. In contrast, the dispersions of Si NCs passivated by allyl disulfide as described above exhibit high chemical and colloidal stability in air, allowing fabrication of optoelectronic devices from them in air. For device fabrication we prepared Si NC ink at a Si concentration of ≈30 mg ml^{-1}, using allyl disulfide as both ligand and solvent. To investigate the viability of Si NC-based photodetectors prepared from this new Si NC ink, we first studied the performance of a simple ITO-Si NC-Al structure. Unfortunately, such devices showed poor photoresponse to simulated solar illumination, even at a relatively high bias of 10 V (Figure S2, Supporting Information). We attribute this to poor charge separation, although a Schottky junction barrier is expected to form at the interface between the Si NC film and Al back electrode. In addition, the weak absorbance of Si NCs, due to the indirect nature of their band gap transitions, leads to the need for a thicker absorber layer compared to direct band gap materials such as lead and cadmium chalcogenides. This negatively impacts the trade-off between absorbance and charge transport distance, which is a key factor determining

© 2014 WILEY-VCH Verlag GmbH & Co. KGaA, Weinheim

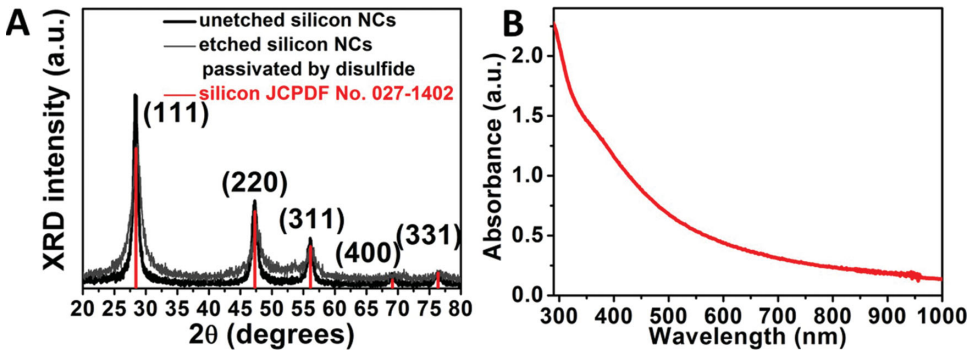

Figure 6. A) Powder XRD of unetched Si NCs, etched Si NCs, and standard XRD pattern of crystalline Si. B) Optical absorbance of Si NCs with 4.5 nm mean size.

performance of nanocrystalline devices. In contrast to conventional monocrystalline Si or polycrystalline Si with relatively large grain size, the film composed of ≈4.5 nm Si NCs possesses a high concentration of interfaces that reduce carrier mobility and promote recombination. The thickness of the NC film significantly impacts the short-circuit current in the device. Device performance can thus be improved by introducing a charge separating layer to improve electron-hole separation. **Figure 7**A shows a schematic of the device structure in which such a layer of poly(3,4-ethylenedioxy-thiophene):poly(styrene sulfonate) (PEDOT:PSS) was added. Scanning electron microscopy (SEM) shows the thickness of the Si NC and PEDOT:PSS layers. The Si NC film has a mean thickness of ≈200 nm while the PEDOT:PSS polymer film was 25 to 30 nm thick. Due to the wide band gap of PEDOT:PSS, and corresponding high conduction band edge, conduction band electrons generated by light absorption in Si NC are blocked by this layer, while holes can be transported to the transparent conductive electrode (Figure 7C). The electron-hole separation is enhanced by the built-in electric field across the interface between Si and Al that drives the electrons toward the Al electrode.

The current-voltage (*J-V*) curves for the device were measured in the dark and under illumination by a standard 100 mW cm^{-2} A.M. 1.5 solar simulator (**Figure 8**A). The open circuit voltage of ≈0.25 V demonstrates photovoltaic behavior and confirms formation of a Schottky barrier at the junction between Si and Al. To test the transient photoresponse, the current density in the device was measured as the light was switched on and off. Note that all of the measurements were carried out in air without any device packaging. Figure 8B shows a high ratio of photocurrent under solar illumination to the dark current (≈700:1) and fast response to light. Moreover, the device performance changed only slightly after tens of cycles, demonstrating the stability of the unpackaged device operating in air. However, the Si NC device has low short-circuit current, which we attribute to the low optical absorption of the silicon NCs. The thickness of the Si NC film (≈200 nm) is not appropriate for use in photovoltaic devices. Crystalline Si solar cells with high power conversion efficiency generally have absorber layers that are several or even several tens of μm thick.[14] Nonetheless, the presence of built-in electric field and photoresponse in the device demonstrated here provide the possibility of making high-performance Si NC-based photodiodes. The spectral responsivity of the device was measured by monitoring the current as the wavelength of incident light was varied (**Figure 9**). No photoresponse was observed for wavelengths longer than 610 nm, consistent with a quantum-confinement induced blue-shift of the indirect band gap energy. The band gap of Si NCs ≈4.5 nm in diameter was estimated using the Tauc method based on the spectral responsivity. The estimated band gap of ≈1.9 eV corresponds well to the results of

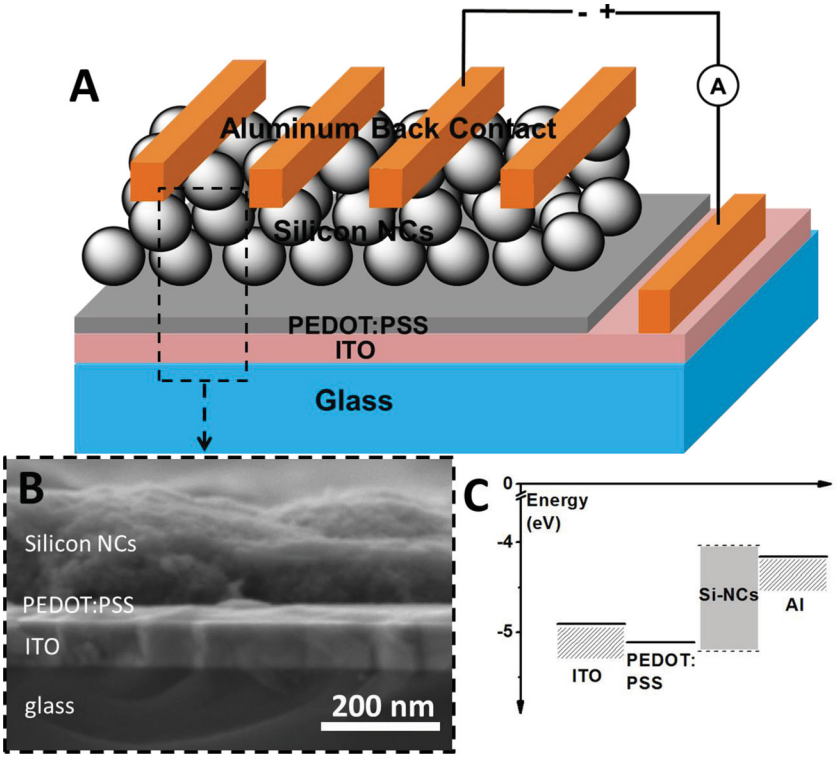

Figure 7. A) Schematic of device structure, B) SEM of the Si NC device, and C) energy band diagram of the materials in this device.

© 2014 WILEY-VCH Verlag GmbH & Co. KGaA, Weinheim

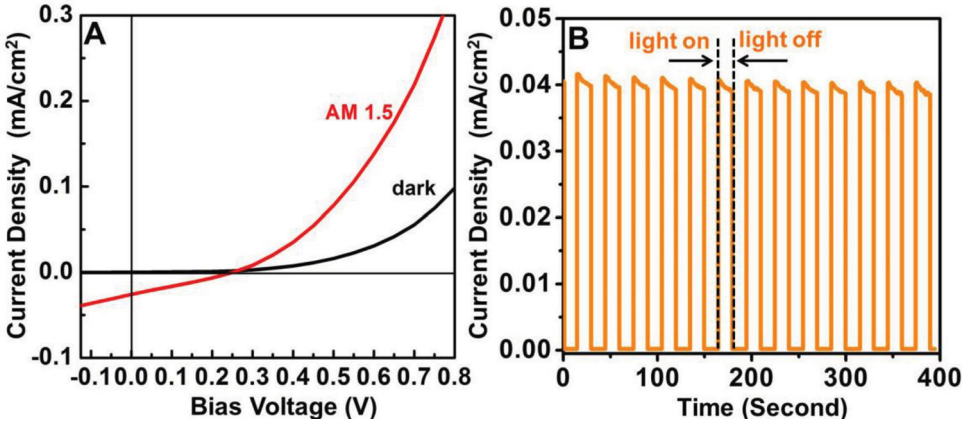

Figure 8. A) Current-voltage scanning and B) transient photoresponse of Si NC device under AM 1.5 simulated solar light.

previous studies of the dependence of the band gap of Si QDs on their size.[13] The photoreponsivity from 950 nm to 600 nm ranged from 10^{-5} to 10^{-4} A W^{-1} (Figure S3, Supporting Information) and the photoresponsivity from 600 nm to 395 nm ranged from 10^{-4} to 10^{-3} AW^{-1}, while the photoresponsivity in the UV spectral region was substantially higher. It reached a maximum value of ≈0.02 AW^{-1} at 310 nm (4 eV) which is two orders of magnitude higher than the responsivity obtained using excitation light near the band-gap energy (≈1.9 eV). Bulk crystalline Si has a direct transition at ≈3.4 eV. Thus, the direct band gap blue-shifted slightly. The wavelength of peak responsivity could potentially be further blue-shifted by reducing the Si NC size. Most commercial UV photodiodes, which are based upon epitaxial films of gallium nitride, silicon carbide, or gallium phosphide, show peak photoresponsivity of 0.1 A W^{-1} or less. Thus, this non-optimized solution-processed device already has comparable sensitivity to conventional UV photodiodes, with the potential to be fabricated over large areas on low-cost, flexible substrates. To test the stability of our devices, we stored them at ambient laboratory conditions and measured the spectral responsivity after 3 weeks. The peak responsivity was ≈0.011 AW^{-1}, within a factor of 2 of the initial responsivity. This demonstrates exceptionally promising air stability for an unpackaged device created from high surface area nanocrystals.

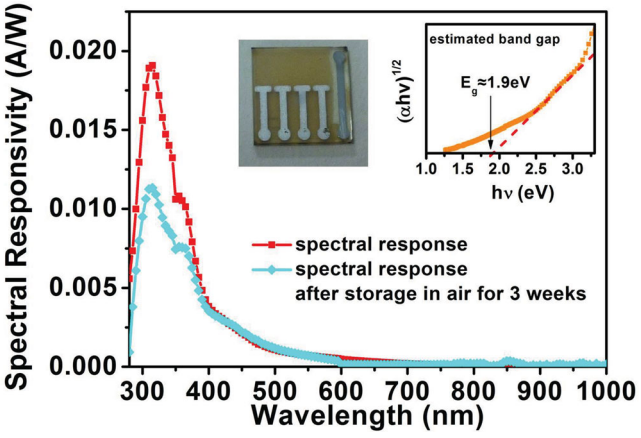

Figure 9. Spectral responsivity of a Si NC device (red curve) and responsivity of the device after storage in air for 3 weeks (blue curve). The inset figure shows the band gap estimated by the Tauc method. The inset photograph shows the Si NC device.

3. Conclusions

In summary, a high-quality Si NC ink was prepared by functionalizing hydrogen-terminated Si NCs using a new type of ligand, namely allyl disulfide. The colloidal Si NCs exhibited high colloidal and chemical stability in air. A Si NC-based photodiode was fabricated from the Si NC ink by spin-coating. A built-in potential was observed in the device, indicating formation of a Schottky-junction barrier that drives charge separation. Moreover, the introduction of an electron-blocking PEDOT:PSS layer significantly enhanced charge separation in the Si device. The maximum responsivity of this device reached ≈0.02 AW^{-1} at 310 nm which is comparable to the responsivity of commercially-available UV photodiodes. In addition, the relatively high deep UV responsivity demonstrates the potential for applications in deep UV detection. This high performance of the photodiode also bodes well for use of allyl disulfide-passivated silicon NCs in more complex devices, such as LEDs or photovoltaics.

4. Experimental Section

Synthesis of Silicon Nanocrystals: The bare silicon NCs were prepared by laser induced pyrolysis of silane (Figure 1, part I), as described in detail in our previous work.[6b] A continuous IR laser beam (Parallax Technology, emitting up to 106 W with wavelength of 10.6 μm) was focused on the center of a six-way cross reactor, above the central reactant inlet within the reactor. The reactant inlet consists of concentric tubes. Silane (at a flow rate of 40 sccm) and hydrogen (at a flow rate of 140 sccm) enter through the inner tube, while pure hydrogen (at a flow rate of 600 sccm) enters through the annular space between the tubes. Silane absorbs the laser energy and is thereby heated. The reaction zone is confined to a small region at the intersection of the laser beam and the silane/hydrogen stream (≈2 mm in diameter). Si NCs grow following the laser induced dissociation of silane molecules in this zone, and stop growing when they leave this zone and rapidly mix with the surrounding unheated gas. Here hydrogen serves to control the growth rate of the crystals. Helium enters the reactor near the end of the four horizontal arms of the six-way cross, confining the reactants and nanocrystals to

© 2014 WILEY-VCH Verlag GmbH & Co. KGaA, Weinheim

a region near the axis of the reactor and preventing the accumulation of particles in the arms of the cross. The aerosol of crystals formed in the reactor flows through a cellulose nitrate membrane filter, where the crystals are collected. This method can produce silicon crystals with a mean size around 15 nm at a rate of 300 mg h^{-1}. The NCs are transferred from the sealed filters to airtight vials in a glove box under nitrogen.

Etching and Surface Modification of Silicon Nanocrystals: In a typical experiment, laser-synthesized silicon NC powder (300 mg) was dispersed in methanol (50 mL) and sonicated (30 min). Then hydrofluoric acid (HF, 100 mL, 48 wt%) and nitric acid (HNO_3, 10 mL, 69 wt%) were added into the mixture. After stirring for 2 min, the cloudy suspension was poured into methanol (400 mL) to slow down the reaction. The etched NCs were collected on a poly(vinylidene fluoride) (PVDF) membrane filter (Durapore from EMD-Millipore, 142 mm in diameter) by pressure filtration. After rinsing with excess methanol, etched NCs (60 mg) were dispersed in allyl disulfide (Aldrich, 2 mL), and sealed in an airtight vial under a nitrogen atmosphere. Then the liquid sample was irradiated in an ultraviolet (UV) reactor with vigorous stirring.

Characterization of Silicon Nanocrystals: TEM images were obtained using a JEOL model JEM 2010 microscope (at an acceleration voltage of 200 kV). A Rigaku Ultima IV X-ray diffractometer was used for X-ray diffraction (XRD) studies. FTIR spectra were measured on a Bruker Vertex 70 spectrometer in attenuated total reflectance mode. UV-Vis absorption spectra were acquired using a Shimadzu UV-3600 spectrophotometer.

Fabrication of Si NC Photodiodes: The indium tin oxide (ITO) coated glass substrates were pre-cleaned using deionized water and acetone, followed by UV-ozone treatment (30 min). Then one layer of PEDOT:PSS (25 to 30 nm in thickness) was fabricated by spin coating. The Si NC thin film was fabricated by spin coating the silicon NC dispersion in allyl disulfide (≈30 mg mL^{-1}) on the PEDOT:PSS layer (spinning rate of 2000 rpm for 38 s). This procedure of depositing Si NC was repeated 10 times to achieve a ≈200 nm thick Si NC film. The Si NC film was annealed at 185 °C for 15 min in an inert atmosphere glove box to remove the residual solvent. An Al layer (70 nm in thickness) was deposited through a mask using an electron beam evaporator, at a deposition rate of 0.6 Å s^{-1} under a background pressure of 5×10^{-7} Torr. The mask used for the back contact produced devices with an active area of 4.25 mm^2.

Photoresponse Measurement of the Photodiode: In order to obtain the full spectral response of the Si NC photodetector, we used a light source (Newport model 5253, 150 Watt Xenon UV Enhanced Arc Lamp) coupled to a wavelength calibrated monochromator (Princeton Instruments Acton Spectropro 2300i, full-width at half-maximum (FWHM) of approximately 0.2 nm). A computerized Keithley 2400 source meter was used for current-voltage measurements. The optical power at each wavelength was measured using a calibrated UV photodetector (DET10A – Si Detector, 200–1100 nm) and pico-ammeter. (KEITHLEY model 6485). All equipment and data acquisition were controlled by Labview. To test the photoresponse to simulated solar light, an A.M. 1.5 solar simulator was used directly. *J–V* scanning and transient photoresponsivity were carried out and measured using a Keithley 2400 source meter.

Supporting Information

Supporting Information is available from the Wiley Online Library or from the author.

Acknowledgements

T.L. and X.L. contributed equally to this work. This work was partially supported by the Korea Institute of Energy Research (Grant No. GP2012–0024–01).

Received: February 20, 2014
Revised: April 12, 2014
Published online: July 25, 2014

[1] a) A. H. Mueller, M. A. Petruska, M. Achermann, D. J. Werder, E. A. Akhadov, D. D. Koleske, M. A. Hoffbauer, V. I. Klimov, *Nano Lett.* **2005**, *5*, 1039; b) V. Wood, M. J. Panzer, J.-M. Caruge, J. E. Halpert, M. G. Bawendi, V. Bulovic, *Nano Lett.* **2009**, *10*, 24; c) K.-Y. Cheng, R. Anthony, U. R. Kortshagen, R. J. Holmes, *Nano Lett.* **2011**, *11*, 1952; d) L. Sun, J. J. Choi, D. Stachnik, A. C. Bartnik, B.-R. Hyun, G. G. Malliaras, T. Hanrath, F. W. Wise, *Nat. Nanotechnol.* **2012**, *7*, 369.

[2] a) I. Gur, N. A. Fromer, M. L. Geier, A. P. Alivisatos, *Science* **2005**, *310*, 462; b) C.-Y. Liu, Z. C. Holman, U. R. Kortshagen, *Nano Lett.* **2008**, *9*, 449; c) J. M. Luther, M. Law, M. C. Beard, Q. Song, M. O. Reese, R. J. Ellingson, A. J. Nozik, *Nano Lett.* **2008**, *8*, 3488; d) J. J. Choi, Y. F. Lim, M. B. Santiago-Berrios, M. Oh, B. R. Hyun, L. F. Sung, A. C. Bartnik, A. Goedhart, G. G. Malliaras, H. D. Abruna, F. W. Wise, T. Hanrath, *Nano Lett.* **2009**, *9*, 3749; e) J. Tang, K. W. Kemp, S. Hoogland, K. S. Jeong, H. Liu, L. Levina, M. Furukawa, X. Wang, R. Debnath, D. Cha, K. W. Chou, A. Fischer, A. Amassian, J. B. Asbury, E. H. Sargent, *Nat. Mater.* **2011**, *10*, 765; f) A. H. Ip, S. M. Thon, S. Hoogland, O. Voznyy, D. Zhitomirsky, R. Debnath, L. Levina, L. R. Rollny, G. H. Carey, A. Fischer, K. W. Kemp, I. J. Kramer, Z. Ning, A. J. Labelle, K. W. Chou, A. Amassian, E. H. Sargent, *Nat. Nanotechnol.* **2012**, *7*, 577; g) S. Ren, L.-Y. Chang, S.-K. Lim, J. Zhao, M. Smith, N. Zhao, V. Bulovic, M. Bawendi, S. Gradecak, *Nano Lett.* **2011**, *11*, 3998.

[3] a) Y. Z. Jin, J. P. Wang, B. Q. Sun, J. C. Blakesley, N. C. Greenham, *Nano Lett.* **2008**, *8*, 1649; b) G. Konstantatos, I. Howard, A. Fischer, S. Hoogland, J. Clifford, E. Klem, L. Levina, E. H. Sargent, *Nature* **2006**, *442*, 180; c) D. C. Oertel, M. G. Bawendi, A. C. Arango, V. Bulovic, *Appl. Phys. Lett.* **2005**, *87*, 213505; d) J. P. Clifford, G. Konstantatos, K. W. Johnston, S. Hoogland, L. Levina, E. H. Sargent, *Nat. Nanotechnol.* **2009**, *4*, 40.

[4] M. Graetzel, R. A. Janssen, D. B. Mitzi, E. H. Sargent, *Nature* **2012**, *488*, 304.

[5] W.-k. Koh, S. R. Saudari, A. T. Fafarman, C. R. Kagan, C. B. Murray, *Nano Lett.* **2011**, *11*, 4764.

[6] a) J. D. Holmes, K. J. Ziegler, R. C. Doty, L. E. Pell, K. P. Johnston, B. A. Korgel, *J. Am. Chem. Soc.* **2001**, *123*, 3743; b) X. G. Li, Y. Q. He, S. S. Talukdar, M. T. Swihart, *Langmuir* **2003**, *19*, 8490; c) L. Mangolini, E. Thimsen, U. Kortshagen, *Nano Lett.* **2005**, *5*, 655; d) D. Neiner, H. W. Chiu, S. M. Kauzlarich, *J. Am. Chem. Soc.* **2006**, *128*, 11016; e) C. M. Hessel, D. Reid, M. G. Panthani, M. R. Rasch, B. W. Goodfellow, J. Wei, H. Fujii, V. Akhavan, B. A. Korgel, *Chem. Mater.* **2011**, *24*, 393; f) Z. Yang, M. Dasog, A. R. Dobbie, R. Lockwood, Y. Zhi, A. Meldrum, J. G. Veinot, *Adv. Funct. Mater.* **2014**, *24*, 1345.

[7] F. Maier-Flaig, J. Rinck, M. Stephan, T. Bocksrocker, M. Bruns, C. Kübel, A. K. Powell, G. A. Ozin, U. Lemmer, *Nano Lett.* **2013**, *13*, 475.

[8] Y. Liu, M. Gibbs, J. Puthussery, S. Gaik, R. Ihly, H. W. Hillhouse, M. Law, *Nano Lett.* **2010**, *10*, 1960.

[9] D. S. Chung, J.-S. Lee, J. Huang, A. Nag, S. Ithurria, D. V. Talapin, *Nano Lett.* **2012**, *12*, 1813.

[10] a) J. M. Luther, M. Law, Q. Song, C. L. Perkins, M. C. Beard, A. J. Nozik, *ACS Nano* **2008**, *2*, 271; b) J.-S. Lee, M. V. Kovalenko, J. Huang, D. S. Chung, D. V. Talapin, *Nat. Nanotechnol.* **2011**, *6*, 348.

[11] L. M. Wheeler, N. R. Neale, T. Chen, U. R. Kortshagen, *Nat. Commun.* **2013**, *4*, 2197.

[12] F. Erogbogbo, T. H. Liu, N. Ramadurai, P. Tuccarione, L. Lai, M. T. Swihart, P. N. Prasad, *ACS Nano* **2011**, *5*, 7950.

[13] T.-W. Kim, C.-H. Cho, B.-H. Kim, S.-J. Park, *Appl. Phys. Lett.* **2006**, *88*, 123102.

[14] a) J. Zhao, A. Wang, M. A. Green, F. Ferrazza, *Appl. Phys. Lett.* **1998**, *73*, 1991; b) J. H. Petermann, D. Zielke, J. Schmidt, F. Haase, E. G. Rojas, R. Brendel, *Prog. Photovoltaics: Res. Appl.* **2012**, *20*, 1.

© 2014 WILEY-VCH Verlag GmbH & Co. KGaA, Weinheim